Journal for Geometry and Graphics
Volume 10 (2006), No. 1, 37–62.

Multifocal Surfaces and Algorithms for Displaying Them

Wilhelm M. Pieper

Fachhochschule Giessen-Friedberg
D 35390 Giessen, Germany
email: wilhelm.m.pieper@mni.fh-giessen.de

Abstract. This article investigates mathematical properties of three-dimensional generalizations of an ellipse (called string surfaces) and a lemniscate (called product surfaces) with more than two foci. They are defined by implicit functions. The singular points of both kinds of surfaces with three foci are calculated analytically. It is explained how the string surfaces can easily be constructed by use of a string. In addition some special cases of surfaces with more than three foci are studied and the transition is made to a continuous distribution of foci. 3D-views of the surfaces with equilateral, linear or isosceles arrangement of the three foci are presented. In Section 4 "axial surfaces" of the form $f(x, y) = c(z)$ are discussed, where the constant c of the 2D-string surfaces $f(x, y)$ is varying with z. Finally a simplification of the polygonization used in the known algorithms for displaying implicit surfaces is described and a new method of radial projection is presented.

Key Words: string surfaces, product surfaces, octree algorithm, iso-surfaces, Cassini surfaces, lemniscate, implicit functions, pseudofocus, Fermat's point, radial projection

MSC 2000: 53A05, 68U05, 51M04

1. Introduction

Let us call a sphere $|\mathbf{x} - \mathbf{x}_1| = R$ a *monofocal surface.*[1] All waves starting from the focus $\mathbf{x}_1$ are reflected by the surface back to the focus. It can be approximated by the use of a stretched string, whose first end is fixed at the focus $\mathbf{x}_1$ and whose second end moves along the surface. In the same way a gardener constructs an ellipse $|\mathbf{x} - \mathbf{x}_1| + |\mathbf{x} - \mathbf{x}_2| = a$ by fixing the ends of a string of length a at the foci $\mathbf{x}_1$ and $\mathbf{x}_2$ and stretching the string to the point $\mathbf{x}$. It's a *bifocal curve.* The rotation of this curve about the axis $\mathbf{x}_1 \vee \mathbf{x}_2$ creates the

[1] Vectors are written by bold face letters in this paper, e.g., $\mathbf{x}$ or $\mathbf{n}$.

ISSN 1433-8157/$ 2.50

bifocal surface of an ellipsoid. Its equation reads

$$f(x,y,z) = \sqrt{(x-x_1)^2+(y-y_1)^2+(z-z_1)^2} + \sqrt{(x-x_2)^2+(y-y_2)^2+(z-z_2)^2} = a\,. \tag{1}$$

One can interpret this formula as an additive blend of two spheres $|\mathbf{x}-\mathbf{x}_i| = R_i$ with $a = R_1 + R_2$. Waves starting from one focus are reflected to the other focus, because the normal of the surface

$$\mathbf{n} = \mathbf{grad}\, f = \frac{\mathbf{x}-\mathbf{x}_1}{|\mathbf{x}-\mathbf{x}_1|} + \frac{\mathbf{x}-\mathbf{x}_2}{|\mathbf{x}-\mathbf{x}_2|} = \mathbf{u}_1 + \mathbf{u}_2 \tag{2}$$

is the sum of two unit vectors $\mathbf{u}_1$ and $\mathbf{u}_2$, i.e., $\mathbf{n}$ is the bisector between the two vectors $\mathbf{x}-\mathbf{x}_1$ and $\mathbf{x}-\mathbf{x}_2$. The normal is needed to calculate the visibility and the illumination of the point $\mathbf{x}$. When the positions $\mathbf{x}_i$ of the two foci are given, then the shortest length a of the large axis of an ellipsoid is $a_{min} = |\mathbf{x}_1 - \mathbf{x}_2|$. In this case the ellipsoid degenerates to a line segment from $\mathbf{x}_1$ to $\mathbf{x}_2$ and all points $\mathbf{x}$ of this line segment have the same sum a_{min} of their distances to the foci.

This article investigates *string surfaces* like

$$f(x,y,z) = |\mathbf{x}-\mathbf{x}_1| + |\mathbf{x}-\mathbf{x}_2| + |\mathbf{x}-\mathbf{x}_3| = c\,, \tag{3}$$

where the *arithmetical* mean value of the distances between a point $\mathbf{x}$ of the surface and the foci $\mathbf{x}_i$ is constant as well as *product surfaces* like

$$f(x,y,z) = |\mathbf{x}-\mathbf{x}_1| \cdot |\mathbf{x}-\mathbf{x}_2| \cdot |\mathbf{x}-\mathbf{x}_3| = c^3, \tag{4}$$

where the corresponding *geometrical* mean value is constant. The product surfaces are multiplicative blends of three spheres written as $|\mathbf{x}-\mathbf{x}_i| = R_i$ with $c^3 = R_1R_2R_3$ (see Section 3), while multiplicative blends of the equation $|\mathbf{x}-\mathbf{x}_i| - R_i = 0$ represent just three spheres. Both can be called *"multifocal surfaces"*, because the distances $|\mathbf{x}-\mathbf{x}_i|$ from the surface point $\mathbf{x}$ to the foci $\mathbf{x}_i$ are either summed up or multiplied. The string surfaces are also called *"iso-surfaces"*, *"iso-potential surfaces"* [7] or *"ellipsoids of order n"* [1], while surfaces where only the distance to the closest focus is taken into account, i.e., $\min_{i=1,..,n} |\mathbf{x}-\mathbf{x}_i| = c$, are called *"distance surfaces"* and the triangle of the foci is called a *skeleton*.

2. String surfaces

If one transforms the "simple" implicit equation (3) into an explicit form, the program "MATHEMATICA" delivers a degree eight expression $z(x,y)$ of the twelve coordinates of the vectors $\mathbf{x}, \mathbf{x}_1, \mathbf{x}_2, \mathbf{x}_3$ with approx. 3500 terms, which is difficult to handle. Therefore the implicit form is used for calculations and rendering.

One can approximate the surface again by the use of a string, if the point $\mathbf{x}$ and the three foci $\mathbf{x}_i$ are represented by small rings. One end of the string is fixed to the ring at $\mathbf{x}$. Then the string passes through the rings at $\mathbf{x}_1, \mathbf{x}_2$ and $\mathbf{x}$ and the other end is finally fixed to the ring at $\mathbf{x}_3$. This path of the string can be described by the notation

$$\mathbf{x} \Rightarrow \mathbf{x}_1 \rightarrow \mathbf{x}_2 \Rightarrow \mathbf{x} \Rightarrow \mathbf{x}_3\,.$$

Here the arrows $\Rightarrow$ describe distances which sum up to the length of the constant c in (3), while the arrow $\rightarrow$ marks a distance which is a constant part of the string that does not contribute to c. In this case the total length of the string has to be $c + |\mathbf{x}_1 - \mathbf{x}_2|$. The ring at $\mathbf{x}$ can be moved around in space to reach all the points of the surface. During this motion the string glides through the rings.

2.1. Trifocal string surfaces

The form of the trifocal surface of (3) depends on the positions $\mathbf{x}_i$ of the three foci and on the constant c. For large values of c and finite $|\mathbf{x}_i|$ it becomes a sphere with $R = |\mathbf{x}| \to c/3$ because $\lim_{|\mathbf{x}|\to\infty} \sum_{i=1}^{3} |\mathbf{x} - \mathbf{x}_i| = 3 \lim_{|\mathbf{x}|\to\infty} |\mathbf{x}|$. Reducing the length of the string makes the surface smaller and smaller until only a singular point $\mathbf{x}_0$ is left, described by its definition:

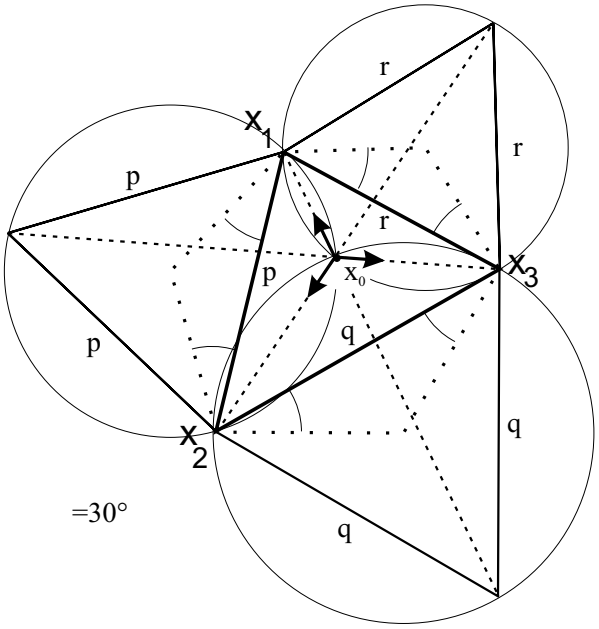

Figure 1: Definition of Fermat's point

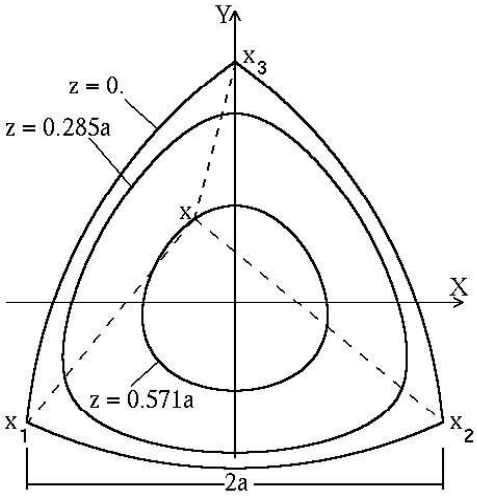

Figure 2: Cuts of a string surface where the three foci form an equilateral triangle

$$\mathbf{n} = \mathbf{grad}\, f = \frac{\mathbf{x} - \mathbf{x}_1}{|\mathbf{x} - \mathbf{x}_1|} + \frac{\mathbf{x} - \mathbf{x}_2}{|\mathbf{x} - \mathbf{x}_2|} + \frac{\mathbf{x} - \mathbf{x}_3}{|\mathbf{x} - \mathbf{x}_3|} = \mathbf{u}_1 + \mathbf{u}_2 + \mathbf{u}_3 = \mathbf{0}. \tag{5}$$

E. Weiszfeld [1, 2] has proved that functions $f(x, y, z) = \sum_{i=1}^{n} |\mathbf{x} - \mathbf{x}_i| = c$ with $n > 2$ foci have only one minimum $\mathbf{x}_0$, but he did neither study nor display the surfaces $f(x, y, z) = \text{const}$. Because of the vector character of the variables Eq. (5) represents three degree twelve equations, whose solutions are called $\mathbf{x}_0 = (x_0, y_0, z_0)$. The sum of three unit vectors $\mathbf{u}_i$ can be zero only if they are coplanar and if the angles between two of them are 120°. Elementary analytical geometry tells us that $\mathbf{x}_0$ can be found as the point of intersection of three circles in Fig. 1 whose centers are defined by the angles $\beta = 30°$. The angles at the three centers are 120° as well as the three angles in $\mathbf{x}_0$ between the vectors $\mathbf{x}_i - \mathbf{x}_0$. It turns out that $\mathbf{x}_0$ is Fermat's point of that triangle. This has to be proved:

Proof: We choose a coordinate system in such a way that

$$\mathbf{x}_1 = (0, 0, 0), \quad \mathbf{x}_2 = (a, 0, 0), \quad \mathbf{x}_3 = (b, d, 0),$$

i.e., the line $\mathbf{x}_1 \vee \mathbf{x}_2$ is used as the x-axis. Since $\cos(30°) = \frac{\sqrt{3}}{2}$ and $|\mathbf{x}_1 - \mathbf{x}_2| = a = p$ (see Figs. 1 and 17), the radius of the (p, p, p)-circle is $R_p = \frac{a}{\sqrt{3}} = \frac{p}{\sqrt{3}}$ and its center has the

coordinates $\left(\frac{a}{2},\ -\frac{a}{2\sqrt{3}},\ 0\right)$. Therefore the equation of this (p,p,p)-circle is

$$\left(x-\frac{a}{2}\right)^2+\left(y+\frac{a}{2\sqrt{3}}\right)^2=\frac{a^2}{3},\quad \text{i.e.,}\quad x^2+y^2-ax+\frac{ay}{\sqrt{3}}=0\,. \tag{6}$$

The origin $\mathbf{x}_1$ and $\mathbf{x}_2$ are points of the circle. In a similar way one can derive the equation of the (r,r,r)-circle through the points $\mathbf{x}_1$ and $\mathbf{x}_3$:

$$x^2+y^2+\frac{xd-yb}{\sqrt{3}}-bx-dy=0\,. \tag{7}$$

These circles intersect at the points $\mathbf{x}_1$ and $\mathbf{x}_0$ which solve the two quadratic equations (6) and (7):

$$x_0=\left(d+\frac{a+b}{\sqrt{3}}\right)\cdot P,\qquad y_0=\left(a-b+\frac{d}{\sqrt{3}}\right)\cdot P, \tag{8}$$

$$P=\frac{a\cdot(d+b\sqrt{3})}{2((a-b)^2+d^2+a(b+d\sqrt{3}))}\,. \tag{9}$$

The (q,q,q)-circle through the points $\mathbf{x}_2$ and $\mathbf{x}_3$ with the radius

$$R_q=\frac{q}{\sqrt{3}}=\frac{|\mathbf{x}_2-\mathbf{x}_3|}{\sqrt{3}}=\sqrt{\frac{d^2+(a-b)^2}{3}}$$

has the equation

$$\left(x-\frac{a+b}{2}-\frac{d}{2\sqrt{3}}\right)^2+\left(y-\frac{d}{2}+\frac{b-a}{2\sqrt{3}}\right)^2-\frac{d^2+(b-a)^2}{3}=0\,. \tag{10}$$

The point $\mathbf{x}_0$ is a solution of this equation, too. So any combination of two of the three quadratic equations (6), (7) and (10) delivers the solution (x_0,y_0): the three circles intersect at one point.

We have to proof now, that this point is a point of the line from $\mathbf{x}_1$ to the opposite corner of the (q,q,q)-triangle. The corner

$$\left(x_c=\frac{a+b+d\sqrt{3}}{2}\,,\ y_c=\frac{d+(a-b)\sqrt{3}}{2}\right)$$

is a solution of the intersection of two circles with the same radius $q=|\mathbf{x}_3-\mathbf{x}_2|=\sqrt{d^2+(b-a)^2}$ around the centers $\mathbf{x}_2$ and $\mathbf{x}_3$:

$$\begin{aligned}(x-a)^2+y^2&=d^2+(b-a)^2 &&\text{(circle centered at } \mathbf{x}_2=(a,0,0))\\ (x-b)^2+(y-d)^2&=d^2+(b-a)^2 &&\text{(circle centered at } \mathbf{x}_3=(b,d,0)).\end{aligned}$$

The point (x_0,y_0) is a point of the line from the origin to this corner since

$$\frac{y_c}{x_c}=\frac{d+(a-b)\sqrt{3}}{a+b+d\sqrt{3}}=\frac{y_0}{x_0}\,. \tag{11}$$

A cyclic renaming of the points $\mathbf{x}_i$ and their coordinates proves that (x_0,y_0) is also a point of the lines from $\mathbf{x}_2$ to the corner of the (r,r,r)-triangle and of the line from $\mathbf{x}_3$ to the corner of

the (p,p,p)-triangle. So it is proved that the function f of Eq. (3) has a minimum in Fermat's point. □

If one of the three angles of the given triangle $\mathbf{x}_1, \mathbf{x}_2, \mathbf{x}_3$ is equal or larger than 120° then $\mathbf{x}_0$ is identical with the vertex of this obtuse angle, i.e., $\mathbf{x}_0$ coincides with a focus. For $d = (b-a)\sqrt{3}$ the angle at $\mathbf{x}_2$ is 120° (see Fig. 17), because $\tan(60°) = \sqrt{3}$ and Eqs. (8) give the point $\mathbf{x}_0 = (a, 0) = \mathbf{x}_2$ as the point of the minimum. If the angle becomes still larger ($d < (b-a)\sqrt{3}$), the point $\mathbf{x}_0$ of intersection of the three circles is outside the triangle $\mathbf{x}_1, \mathbf{x}_2, \mathbf{x}_3$ and is not a solution of Eq. (5) anymore, because the angles between the $\mathbf{u}_i$ are 60°, 60°, and 120°, respectively.

For example, if $d = a$ and $b = 2a$, the angle at $\mathbf{x}_2$ is $90° + 45° = 135°(> 120°)$ and we find: $\mathbf{x}_0 = (0.9058\,a,\ -0.1401\,a)$ which is outside the $\mathbf{x}_i$-triangle since $y_0 < 0$. It is obvious that

$$f(\mathbf{x}_0) = |\mathbf{x}_0 - \mathbf{x}_1| + |\mathbf{x}_0 - \mathbf{x}_2| + |\mathbf{x}_0 - \mathbf{x}_3| > f(\mathbf{x}_2) = |\mathbf{x}_2 - \mathbf{x}_1| + 0 + |\mathbf{x}_2 - \mathbf{x}_3|.$$

This is true for all points $\mathbf{x}_0$ outside the triangle. Therefore one can say that the point of the minimum of f is given by Eqs. (8) if every angle α_i of the triangle is smaller than or equal to 120° and that the minimum is in $\mathbf{x}_i$ if $\alpha_i > 120°$.

Fig. 2 shows the curves of the intersections of the planes $z = \text{const.}$ with a trifocal surface, in which the foci

$$\mathbf{x}_1 = \left(-a,\ -\frac{a}{\sqrt{3}},\ 0\right), \quad \mathbf{x}_2 = \left(a,\ -\frac{a}{\sqrt{3}},\ 0\right), \quad \mathbf{x}_3 = \left(0,\ \frac{2a}{\sqrt{3}},\ 0\right)$$

form an equilateral triangle with sides of length $s = 2a$ and the string has the length $f(\mathbf{x}_i) = c = s + 0 + s = 4a$ (see Eq. (3)) to make sure that the foci are points of the surface. In this symmetric surface Fermat's point is the center of the triangle $\mathbf{x}_0 = (0,0,0)$. The top and bottom of it are the points $(0,0,\pm\frac{s}{3})$. The curves of Fig. 2 are the intersections with the planes $z_1 = 0$, $z_2 = 0.285\,a$ and $z_3 = 0.571\,a$. The z_1-intersection looks like a Releaux-triangle, but is different.

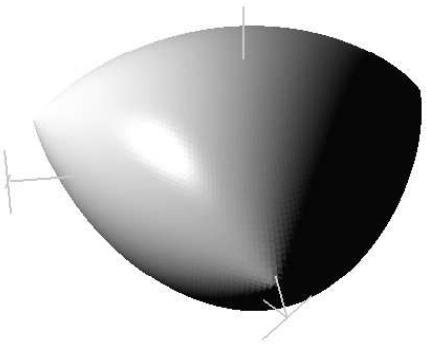

Figure 3: 3D-view of the surface of Fig. 2

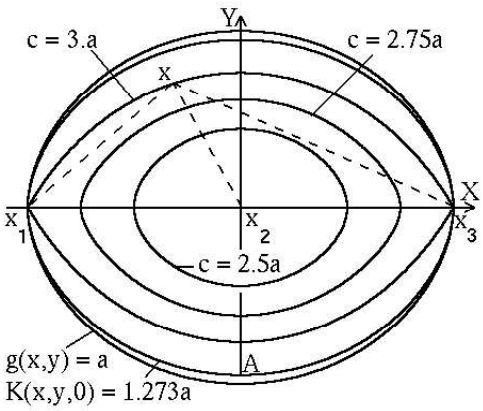

Figure 4: ($z=0$)-cuts of string surfaces defined by (12), (26) and (29)

A 3D-view of the surface is shown in Fig. 3. The foci can be recognised in the silhouette. The string construction of this surface may have a technical application, because the ring of point $\mathbf{x}$ moves to the point $\mathbf{x}_0$ from every point in the space, if one pulls at the end of the string in the remote point $\mathbf{x}_3$.

Another trifocal surface was studied with a linear arrangement of the foci on the x-axis: $\mathbf{x}_1 = (-a, 0, 0)$, $\mathbf{x}_2 = (0, 0, 0)$, $\mathbf{x}_3 = (a, 0, 0)$ (see Fig. 4):

$$\sqrt{(x+a)^2 + y^2 + z^2} + \sqrt{x^2 + y^2 + z^2} + \sqrt{(x-a)^2 + y^2 + z^2} - c = 0\,. \tag{12}$$

The surface is symmetrical with the x-axis as the axis of rotation. Since the second focus is a point of the line $\mathbf{x}_1 \vee \mathbf{x}_3$, the shortest string length is $c = |\mathbf{x}_1 - \mathbf{x}_3| = 2a$. With this c-value the surface degenerates to a point: $\mathbf{x}_0 = \mathbf{x}_2$. Squaring (12) several times leads to a degree eight equation for $z = 0$:

$$16c^2\left((x+a)^2 + y^2\right)\left(c^2 + 4ax - x^2 - y^2\right)^2 - \left((c^2 + x^2 + y^2 + 2a^2)^2 + 4c^2\left((x+a)^2 + y^2\right)\right.$$
$$\left. -4\left((x-a)^2 + y^2\right)\left(c^2 + (x+a)^2 + y^2\right)\right)^2 = 0\,,$$

which can be solved by "MATHEMATICA", but the explicit function of the curve $y(x)$ contains approx. 1500 terms. Therefore another approach was used. In (12) the variables y and z occur only in a combination of the form $x^2 + y^2 + z^2 = r^2$:

$$r + \sqrt{r^2 + a^2 - 2ax} + \sqrt{r^2 + a^2 + 2ax} - c = 0\,. \tag{13}$$

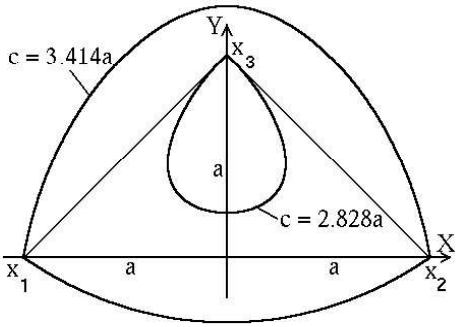

Figure 5: ($z=0$)-cuts of string surfaces where the three foci form a rectangular triangle

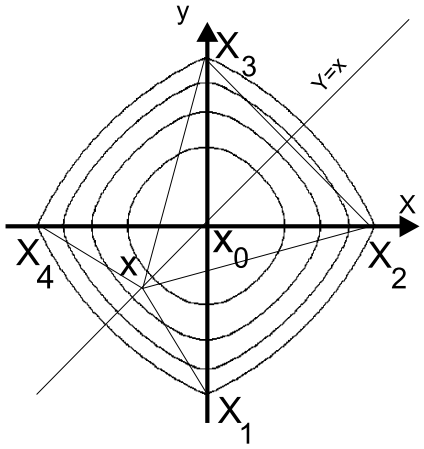

Figure 6: Quadrifocal string surface where the foci form a square

This leads to the parameter representation:

$$x = \pm\frac{c-r}{4a}\sqrt{4(r^2+a^2) - (r-c)^2}\,; \quad y = \sqrt{r^2 - x^2}\cos\phi\,; \quad z = \sqrt{r^2 - x^2}\sin\phi \tag{14}$$

within the region

$$-\frac{c}{3} + \frac{2}{3}\sqrt{c^2 - 3a^2} \le r \le c - 2a \quad \text{and} \quad 0 \le \phi \le 2\pi\,.$$

For $c_0 \neq 3a$ the curves have ellipsoidal shape, but for $c_0 = 3a$ the curve intersects the x-axis at the foci $x = \pm a$ with the slope

$$\beta = \arctan\left(\frac{\partial y}{\partial x}\right) = \arctan\left(\frac{\partial y}{\partial r}/\frac{\partial x}{\partial r}\right) = \arctan\left(\sqrt{\frac{21}{8}}/1\right) = 58.316^\circ.$$

Therefore the c_0-surface can be approximated in the neighbourhood of the two foci by cones with a 2β-angle at their apex. Fig. 4 shows the $(z=0)$-intersections of different surfaces: $c = 2.5\,a$, $2.75\,a$ and $3.0\,a$. The three lines $\mathbf{x} \vee \mathbf{x}_i$ are drawn for one point $\mathbf{x}$ of the $(c = 3.0\,a)$-surface.

In Fig. 5 the three foci form an isosceles rectangular triangle

$$\mathbf{x}_1 = (-a, 0, 0), \quad \mathbf{x}_2 = (a, 0, 0), \quad \mathbf{x}_3 = (0, a, 0).$$

For $\mathbf{x} = \mathbf{x}_1$ the sum of the three distances $|\mathbf{x} - \mathbf{x}_i|$ is

$$0 + 2a + a\sqrt{2} = a\left(2 + \sqrt{2}\right) = 3.414214\,a = c_1\,.$$

The same is true for $\mathbf{x} = \mathbf{x}_2$, but not for $\mathbf{x} = \mathbf{x}_3$. Therefore the foci $\mathbf{x}_1$ and $\mathbf{x}_2$ lie on the c_1-surface but $\mathbf{x}_3$ does not. The surface on which $\mathbf{x}_3$ is lying has the string length $0 + a\sqrt{2} + a\sqrt{2} = 2.828428\,a = c_2$. According to Eqs. (8) Fermat's point is $\mathbf{x}_0 = \left(0,\, \frac{a}{\sqrt{3}},\, 0\right)$ and it is independent of the position b of $\mathbf{x}_3 = (0, b, 0)$ on the y-axis, since a motion of $\mathbf{x}_3$ along the y-axis does not change the three 120°-angles between the vectors $\mathbf{x}_1 - \mathbf{x}_0$, $\mathbf{x}_2 - \mathbf{x}_0$, $\mathbf{x}_3 - \mathbf{x}_0$ at $\mathbf{x}_0$, by which $\mathbf{x}_0$ is defined in Eq. (5). The curve $z(y)$ of the intersection of the $(x=0)$-plane with a trifocal surface can be solved explicitly if the foci represent an isosceles triangle $(\mathbf{x}_i = (\pm a, 0, 0),\ (0, b, 0))$ because in this case two of the three square roots in (3) are equal for $x = 0$:

$$2\sqrt{a^2 + y^2 + z^2} + \sqrt{(y-b)^2 + z^2} = c\,. \tag{15}$$

This is a biquadratic equation for z with the solution

$$z(y) = \pm\sqrt{c^2 + 4(b^2 + c^2 - 3a^2) - (b+3y)^2 - 4c\sqrt{b^2 + c^2 - 3a^2 + 2b(b-3y)}}. \tag{16}$$

It has a vertex in $\mathbf{x}_3$ as shown in Fig. 5 if $\mathbf{x}_3$ is a point of the surface, i.e., if $c = 2\sqrt{a^2 + b^2}$.

2.2. Multifocal string surfaces

In this subsection two special surfaces with four foci are studied. Fig. 6 shows the horizontal $(z=0)$-intersections of surfaces with a quadratic arrangement of the four foci

$$\mathbf{x}_i = (0, -a, 0),\ (a, 0, 0),\ (0, a, 0),\ (-a, 0, 0)$$

where one string is chosen so long that the four foci lie on the surface $c_4 = 0 + 2a + 2\sqrt{2}\,a = 4.828428\,a$. The intrinsic curves correspond to $(z=0)$-cuts of surfaces with smaller strings $c = 4.2071\,a,\ 4.4142\,a,\ 4.6213\,a$. For $c = 4a$ these surfaces shrink to a point $\mathbf{x}_0$. It is the origin of the coordinate system for which the sum of the distances to the four foci is minimal: $c_{min} = 4a$, because (18) gives $\mathbf{grad}\, f = \mathbf{0}$ for $\mathbf{x} = \mathbf{0}$ and $\mathbf{x}_1 = -\mathbf{x}_3$ and $\mathbf{x}_2 = -\mathbf{x}_4$. It

corresponds to Fermat's point of a triangle. If the ends of the string are fixed to the points $\mathbf{x}_1$ and $\mathbf{x}_4$ — as shown in Fig. 6 — the string notation is

$$\mathbf{x}_1 \Rightarrow \mathbf{x} \Rightarrow \mathbf{x}_2 \rightarrow \mathbf{x}_3 \Rightarrow \mathbf{x} \Rightarrow \mathbf{x}_4\,.$$

For a point $\mathbf{x}$ in the plane $y = x$ the four distances in $f(\mathbf{x})$ are equal two by two:

$$|\mathbf{x}-\mathbf{x}_1| = |\mathbf{x}-\mathbf{x}_4| \quad \text{and} \quad |\mathbf{x}-\mathbf{x}_2| = |\mathbf{x}-\mathbf{x}_3|,$$

i.e.,

$$f = 2|\mathbf{x}-\mathbf{x}_1| + 2|\mathbf{x}-\mathbf{x}_2| = c_4\,.$$

This is an equation of an ellipsoid $|\mathbf{x}-\mathbf{x}_1| + |\mathbf{x}-\mathbf{x}_2| = c_4/2 = a(1+\sqrt{2})$ with the foci $\mathbf{x}_1$ and $\mathbf{x}_2$. The same is true for the ellipsoid on the other side of the of the $(y=x)$-plane: $|\mathbf{x}-\mathbf{x}_4| + |\mathbf{x}-\mathbf{x}_3| = a(1+\sqrt{2})$. The cut of both ellipsoids by the plane $y = x$ creates an ellipse. One of its semiaxes $\bar{z} = \frac{a}{2}\sqrt{2\sqrt{2}-1} = 0.6761\,a$ is the solution of the equation $f(0,0,\bar{z}) = 0$. The cartesian coordinate $\bar{x}$ of the second maximum of the ellipse is calculated from $f(\bar{x},\bar{x},0) = 0$: $\bar{x} = a\frac{3+\sqrt{2}}{\sqrt{28}}$. The corresponding semiaxis in the line $(z = 0,\ y = x)$ has the length $\bar{x}\sqrt{2} = 0.8342\,a$. During the motion of the ring $\mathbf{x}$ along the surface in the $(x=y)$-plane the constant part $\mathbf{x}_2 \rightarrow \mathbf{x}_3$ of the string does not move for the simple reason of symmetry. It seems to be fixed at the foci $\mathbf{x}_2$ and $\mathbf{x}_3$. The symmetry of the surface is also the reason why we find the same ellipse in the $(y=-x)$-plane. The segments of the c_4-curve can again be approximated by segments of circles. The c_4-surface looks like a pillow and has the height $\pm\bar{z}$ (see Fig. 7).

In Fig. 20 the term $|\mathbf{x}-\mathbf{x}_5|$ of a fifth focus with $\mathbf{x}_5 = (0,\,0,\,a/4)$ is subtracted from the f-function of the "pillow" of Fig. 7:

$$f_0 = \sum_{i=1}^{4} |\mathbf{x}-\mathbf{x}_i| - |\mathbf{x}-\mathbf{x}_5| = c_5 \quad \text{with} \quad c_5 = c_4 - |\mathbf{x}_1-\mathbf{x}_5| = c_4 - \sqrt{a^2+\left(\frac{a}{4}\right)^2} = 3.7976\,a\,,$$

to make sure that the $\mathbf{x}_i$ are points of f_0. It creates a "dip" in the "pillow".

In Fig. 8 the four foci are not coplanar anymore as in Figs. 6 and 7 but form a symmetrical tetrahedron

$$\mathbf{x}_1 = \left(-\frac{a}{2}\sqrt{3},\ -\frac{a}{2},\ 0\right), \quad \mathbf{x}_2 = \left(\frac{a}{2}\sqrt{3},\ -\frac{a}{2},\ 0\right), \quad \mathbf{x}_3 = (0,a,0), \quad \mathbf{x}_4 = (0,0,b).$$

Its base is a regular triangle. Here the point $\mathbf{x}_0$ of minimal string length c can be calculated analytically, because for reasons of symmetry it has to be a point of the z-axis:

$$f(0,0,z) = \sum |\mathbf{x}-\mathbf{x}_i| = b - z + 3\sqrt{\left(\frac{a}{2}\sqrt{3}\right)^2 + \left(\frac{a}{2}\right)^2 + z^2} = b - z + 3\sqrt{a^2+z^2}$$

and the condition $\mathbf{grad}\, f = \mathbf{0}$ is reduced to $\frac{\partial f}{\partial z} = 0 = -1 + \frac{3z}{\sqrt{a^2+z^2}}$. The solution $z_0 = \frac{a}{2\sqrt{2}}$ is independent of the height b of the tetrahedron, because for $\mathbf{x} = \mathbf{x}_0$ the unit vector $\mathbf{u}_4$ in (19) is independent of b. The f-values grow with increasing b, but their minimum stays in place $\mathbf{x}_0 = (0,0,z_0)$. Fig. 8 shows the string surface of a regular tetrahedron

$$b = a\sqrt{2}, \quad c = 0 + 3|\mathbf{x}_3-\mathbf{x}_4| = 0 + 3\sqrt{a^2+b^2} = 3a\sqrt{3}\,.$$

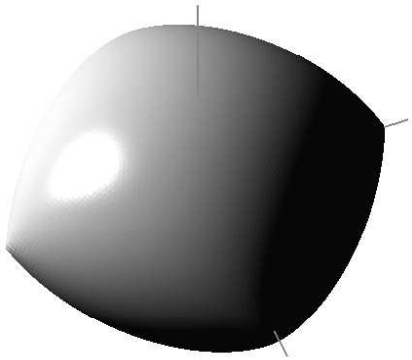

Figure 7: A string surface with a quadratic arrangement of the four foci

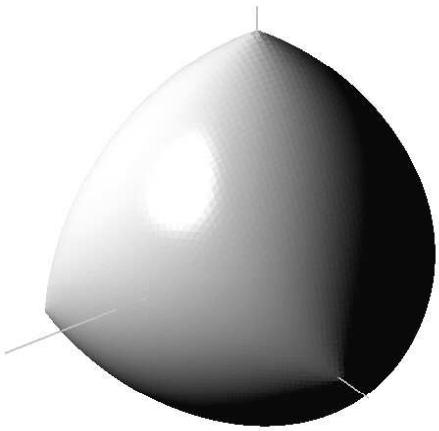

Figure 8: A string surface with a tetrahedral arrangement of the four foci

The camera was put in a position from where three of its four vertices were visible. If the tetrahedron degenerates to a plane, i.e., if the four foci form an (irregular) quadrilateral, then the point $\mathbf{x}_0$ of minimal string length c is the point of intersection of the two diagonals.

Proof: Let us assume that the irregular quadrilateral is convex and that the numeration of the points is clockwise or anticlockwise with the diagonals $\mathbf{x}_1 \vee \mathbf{x}_3$ and $\mathbf{x}_2 \vee \mathbf{x}_4$. Then the sum $|\mathbf{x}-\mathbf{x}_1|+|\mathbf{x}-\mathbf{x}_3|$ is minimal for points $\mathbf{x}$ of the first diagonal and its value is $|\mathbf{x}_1-\mathbf{x}_3|$. The same is true for points of the other diagonal with the value $|\mathbf{x}_2-\mathbf{x}_4|$. Therefore the only point where both sums are minimal is the point $\mathbf{x}_0$ of the intersection of the two diagonals with the minimum $f_{min} = |\mathbf{x}_1-\mathbf{x}_3|+|\mathbf{x}_2-\mathbf{x}_4|$ (see (17)). It is a solution of (19) with $\mathbf{grad}\, f = \mathbf{0}$. □

In general the string surface of four foci

$$f(\mathbf{x}) = \sum_{i=1}^{4} |\mathbf{x}-\mathbf{x}_i| = c \tag{17}$$

has the normal

$$\mathbf{n} = \mathbf{grad}\, f = \sum_{i=1}^{4} \frac{\mathbf{x}-\mathbf{x}_i}{|\mathbf{x}-\mathbf{x}_i|} = \sum_{i=1}^{4} \mathbf{u}_i\,, \tag{18}$$

and the singular point $\mathbf{x}_0$ of the minimum of f is a solution of the three equations

$$\mathbf{n} = \sum_{i=1}^{4} \frac{\mathbf{x}-\mathbf{x}_i}{|\mathbf{x}-\mathbf{x}_i|} = \sum_{i=1}^{4} \mathbf{u}_i = 0 \tag{19}$$

which are degree eight polynomials with approx. 2000 terms if one removes the square roots of the denominators. Eq. (19) can be rewritten

$$\mathbf{u}_1 + \mathbf{u}_2 = -\mathbf{u}_3 - \mathbf{u}_4 \tag{20}$$

and squared

$$1 + 1 + 2\mathbf{u}_1 \cdot \mathbf{u}_2 = 1 + 1 + 2\mathbf{u}_3 \cdot \mathbf{u}_4 \,. \tag{21}$$

This means for the angles between the $\mathbf{u}_i$-vectors that

$$\angle(\mathbf{x}_0 - \mathbf{x}_1, \mathbf{x}_0 - \mathbf{x}_2) = \angle(\mathbf{x}_0 - \mathbf{x}_3, \mathbf{x}_0 - \mathbf{x}_4) \tag{22}$$

or as an abbreviation

$$\phi_{12} = \phi_{34}, \quad \phi_{13} = \phi_{24}, \quad \phi_{14} = \phi_{23} \,. \tag{23}$$

The last two equations are a consequence of permutations of (20). Eq. (23) says that opposite edges of the tetrahedron appear to an observer in $\mathbf{x}_0$ under the same angle and (20) tells in addition that the bisectors of these angles are collinear. It seems that (19) has to be solved numerically for irregular tetrahedra. Its solution $\mathbf{x}_0$ can easily be found by a numerical algorithm starting from an arbitrary point $\mathbf{x}_j$ and running in small steps dx into the direction of $-\mathbf{n}(\mathbf{x})$: $\mathbf{x}_{j+1} = \mathbf{x}_j - \mathbf{n}(\mathbf{x}_j)\, dx$. E. Weiszfeld [1] has given a similar algorithm.

2.3. Convolution surfaces

Eqs. (17), (18) and (19) can be generalized to n foci and one can study the case $n \to \infty$:

$$g(\mathbf{x}) = \frac{1}{V} \int\limits_V \rho(\mathbf{v}) |\mathbf{x} - \mathbf{v}| \, dv = \text{const.} \tag{24}$$

One can call the function $\rho(\mathbf{v})$ a focal density and one can compare this integral with the fundamental equation of the potential theory

$$\Phi(\mathbf{x}) = \frac{1}{V} \int\limits_V \frac{\rho(\mathbf{v}) dv}{|\mathbf{x} - \mathbf{v}|} \,, \tag{25}$$

where $\rho(\mathbf{v})$ is either the charge- or the mass-distribution. The integral (24) can be solved for a constant density $\rho = 1$ if the infinite number of foci forms a straight line $-a \le x_1 \le a$ in x_1-direction:

$$\begin{aligned} g(x,y) &= \frac{1}{2a} \int\limits_{-a}^{a} |\mathbf{x} - \mathbf{x}_1| dx_1 = \frac{1}{2a} \int\limits_{-a}^{a} \sqrt{(x - x_1)^2 + y^2}\, dx_1 \\ &= \frac{1}{4a} \Bigg((a - x)\sqrt{(x-a)^2 + y^2} + (x + a)\sqrt{(x+a)^2 + y^2} \\ &\quad + \; y^2 \ln \left(\frac{a - x + \sqrt{(x-a)^2 + y^2}}{-x - a + \sqrt{(x+a)^2 + y^2}} \right) \Bigg) \quad \text{for} \quad y \neq 0 \,, \\ &= \frac{x^2 + a^2}{2a} \quad \text{for} \quad y = 0 \quad \text{and} \quad |x| \le a \,, \\ &= |x| \quad \text{for} \quad y = 0 \quad \text{and} \quad |x| > a \,. \end{aligned} \tag{26}$$

This leads to the trivial results that the center of the line has a mean distance of $g(0,0) = a/2$ from the line and that the end of the line has a distance of $g(a,0) = a$. To ask for other points with this mean distance (a) means to demand $g(x,y) = a = \text{const}$. This curve is plotted in Fig. 4. A rotation of $g(x,y)$ about the x-axis generates a surface of constant mean distance from the line $\mathbf{x}_1 \vee \mathbf{x}_3$, while a cylinder is a surface with constant minimal distance from its axis. The reader may replace y^2 by $y^2 + z^2$ in (26) to get the function $g(x,y,z)$ of this surface.

Supposed it is asked for a surface, whose mean distance c to four lines should be constant, which form a planar or skew quadrilateral. This can be done by demanding, that the sum

$$G(x,y,z) = \sum_{i=1}^{4} g_i(x,y,z) = c \tag{27}$$

should be constant, which corresponds to the transition from Eq. (1) to (3). — The local coordinates of (26) have to be transformed to common coordinates for every line in (27). —

In Computer Graphics the lines of (27) or the points $\mathbf{x}_i$ in (17) are called *"skeletons"* [3, 4]. The name used in Constructive Solid Geometry (CSG) [5] for such surfaces is *"offset solid"*. In these applications similar surfaces — called *"distance surfaces"* — are studied where the condition

$$\min(g_1, g_2, \ldots, g_n) = \text{const.} \tag{28}$$

keeps the distance to the closest skeleton constant. Another possibility to emphasize the distances $|\mathbf{x} - \mathbf{x}_i|$ to the closest skeleton was proposed by J.F. Blinn [6] for *"iso-potential surfaces"*

$$f(\mathbf{x}) = \sum_{i=1}^{n} \exp\left(-\frac{|\mathbf{x} - \mathbf{x}_i|^2}{2}\right).$$

J. Bloomenthal and K. Shoemake [7] did the transition $n \to \infty$ and analysed *"convolution surfaces"* by replacing the summation of the last equation by an integration. J. Bloomenthal and B. Wyvill [15] used negative terms $-|\mathbf{x} - \mathbf{x}_i|$ to create surfaces with dips, i.e., such foci are "repulsive" to the surface (see Fig. 20), while foci with positive terms $+|\mathbf{x} - \mathbf{x}_i|$ are attractive and create apices (see Figs. 2 to 8).

Unfortunately the attempt to calculate a curve or a surface on which the mean distance to a circle $(r_1 \cos\phi,\ 0,\ r_1 \sin\phi)$ is constant leads to an elliptical integral

$$K(x,y,z) = \frac{1}{2\pi} \int_0^{2\pi} |\mathbf{x} - \mathbf{x}_1|\, d\phi_1 = \frac{1}{2\pi} \int_0^{2\pi} \sqrt{(r_1 \cos\phi_1 - x)^2 + y^2 + (r_1 \sin\phi_1 - z)^2}\, d\phi_1\,. \tag{29}$$

The function K has rotational symmetry with respect to the y-axis of the circle. Fig. 4 shows the curve $K(x,y,0) = a$ obtained by numerical integration of (29) (cf. [8]). The $(y{=}0)$-plane of the circle is perpendicular to the $(z{=}0)$-plane of this paper, and the circle penetrates it in the points $x = \pm r_1 = \pm a$. A rotation of the curve $K(x,y,0) = a$ about the y-axis $A \vee \mathbf{x}_2$ generates a surface, whose points $\mathbf{x}$ have a constant arithmetical mean distance a from the circle.

3. Product surfaces

Bifocal product curves

$$f = |\mathbf{x} - \mathbf{x}_1| \cdot |\mathbf{x} - \mathbf{x}_2| = c^2 \quad \text{or} \quad f^2 = (\mathbf{x} - \mathbf{x}_1)^2 \cdot (\mathbf{x} - \mathbf{x}_2)^2 = c^4 \tag{30}$$

were studied in the seventeenth century by J.D. Cassini. If one reads the $\mathbf{x}$-variables as three-dimensional vectors then (30) represents a surface of revolution with the line $\mathbf{x}_1 \vee \mathbf{x}_2$ as the axis of rotation and with the normal

$$\mathbf{n} = \tfrac{1}{2}\,\mathbf{grad}\, f^2 = f\ \mathbf{grad}\, f = (\mathbf{x} - \mathbf{x}_1)(\mathbf{x} - \mathbf{x}_2) f^2 + (\mathbf{x} - \mathbf{x}_2)(\mathbf{x} - \mathbf{x}_1) f^2. \tag{31}$$

For $c^2 \to 0$ one of the two factors in (30) has to vanish: $\mathbf{x} \to \mathbf{x}_1$ or $\mathbf{x} \to \mathbf{x}_2$, i.e., the curves (or surfaces) split into two parts — one around each focus. Both parts grow in volume with an increasing value of c. There is a particular c-value $c_0 = |\mathbf{x}_1 - \mathbf{x}_2|/2$, where both parts get into contact at the point $\mathbf{x}_0 = (\mathbf{x}_1 + \mathbf{x}_2)/2$. This point is a singular point with $\mathbf{n}_0 = \mathbf{grad}\, f = \mathbf{0}$. The c_0-curve is called a *lemniscate*. It looks like the number "8".

3.1. Trifocal product surfaces

A trifocal product surface

$$\begin{aligned} f(x,y,z) = \textstyle\prod_{i=1}^{3} \sqrt{(x-x_i)^2 + (y-y_i)^2 + (z-z_i)^2} &= c^3 \quad \text{or} \\ F(x,y,z) = f^2(x,y,z) = \textstyle\prod_{i=1}^{3} (\mathbf{x}-\mathbf{x}_i)^2 &= c^6 \end{aligned} \tag{32}$$

splits into three parts for small values of c as shown in Fig. 9. In this case one of the square roots has to be small: $\mathbf{x} \to \mathbf{x}_i$, $i = 1$ or 2 or 3. The foci $\mathbf{x}_i$ are the points of the absolute minima of the function $f(\mathbf{x}_i) = c^3_{min} = 0$. With increasing c the different parts melt together at one or two singular points $\mathbf{x}_{01}$ and/or $\mathbf{x}_{02}$, which are called *"contact points"* in this paper. Their positions depend on the positions $\mathbf{x}_i$ of the foci which influence the number of solutions of their defining equation

$$\begin{aligned} \mathbf{n} = \tfrac{1}{2}\, \mathbf{grad}\, F = f\, \mathbf{grad}\, f = (\mathbf{x}-\mathbf{x}_1)(\mathbf{x}-\mathbf{x}_2)^2(\mathbf{x}-\mathbf{x}_3)^2 \\ + (\mathbf{x}-\mathbf{x}_2)(\mathbf{x}-\mathbf{x}_1)^2(\mathbf{x}-\mathbf{x}_3)^2 + (\mathbf{x}-\mathbf{x}_3)(\mathbf{x}-\mathbf{x}_1)^2(\mathbf{x}-\mathbf{x}_2)^2 = 0\,. \end{aligned} \tag{33}$$

This is a system of three degree five equations for the variables x, y and z.

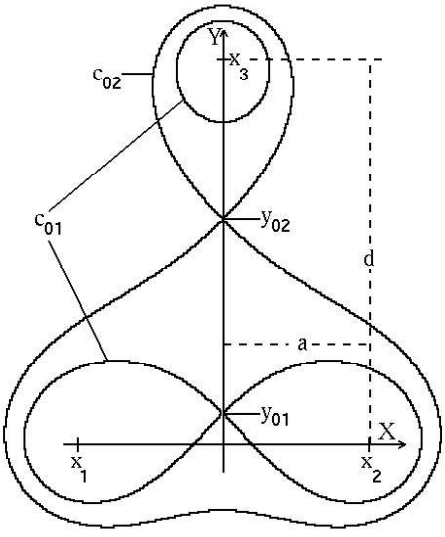

Figure 9: ($z=0$)-cuts of product surfaces with an isosceles focal triangle

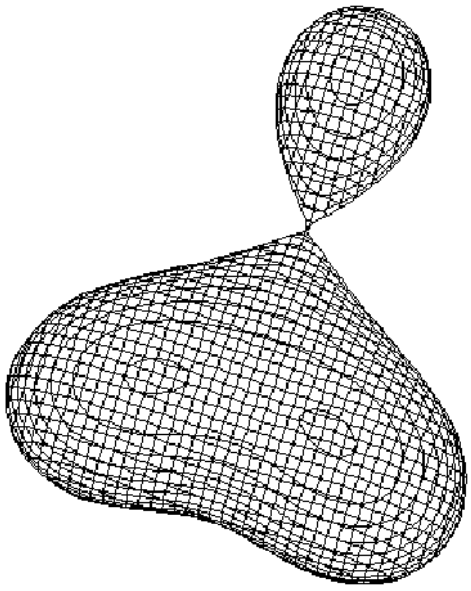

Figure 10: 3D-view of the c_{02}-surface of Fig. 9

The singular contact points $\mathbf{x}_{01}$ and $\mathbf{x}_{02}$ and — due to the factor f — the three foci are solutions of these three equations. In an ε-neighbourhood of a contact point $\mathbf{x}_{0i}$ there are points with $f(\mathbf{x}) < f(\mathbf{x}_{0i})$ belonging to different parts of the surface with $c < c_{0i}$, other points

of the contact surface $f(\mathbf{x}) = c_{0i}$ and points with $f(\mathbf{x}) > c_{0i}$ belonging to the joint surface with $c > c_{0i}$. Therefore the second order term of a Taylor expansion of f in $\mathbf{x}_{0i} = (x_{1,0i},\, x_{2,0i},\, x_{3,0i})$ is indefinite:

$$\begin{aligned} f(\mathbf{x}) &= f(\mathbf{x}_{0i}) + \tfrac{1}{2} \sum_{j,k=1}^{3} \frac{\partial^2 f}{\partial x_j \partial x_k} (x_j - x_{j,0i})(x_k - x_{k,0i}) \\ &= f(\mathbf{x}_{0i}) + \tfrac{1}{2} \sum_{j,k=1}^{3} f_{jk} (x_j - x_{j,0i})(x_k - x_{k,0i}), \end{aligned} \tag{34}$$

i.e., its sign depends on the direction of $\mathbf{x} - \mathbf{x}_{0i}$. The first order term vanishes in $\mathbf{x}_{0i}$ with $\mathbf{grad}\, f = \mathbf{0}$. — Here the variables x, y, z are replaced by x_1, x_2, x_3 and $f_{j,k}$ are the second derivatives, e.g., f_{23} is f_{yz}.— In a contact point the surface resembles an apex of a cone or a multi-cone (see Figs. 9, 10, 14 and 16).

For solving the Eqs. (33), the plane of the three foci is chosen as the $(z=0)$-plane and the coordinate system is placed in such a position that the foci have the coordinates

$$\mathbf{x}_1 = (0, 0, 0), \quad \mathbf{x}_2 = (a, 0, 0), \quad \mathbf{x}_3 = (b, d, 0)$$

(see Fig. 17). Then the contact points lie on the $(z=0)$-plane too: $z_{01} = z_{02} = 0$, because the $(z=0)$-plane is a plane of symmetry: (32) does not depend on the sign of z for $z_i = 0$.

If one substitutes the coordinates of the $\mathbf{x}_i$ into (33) and eliminates one of the three terms by calculating the (weighted) differences of these equations one gets two cubic equations:

$$(dx - by)\left((x-a)^2 + y^2\right) - ay\left((x-b)^2 + (y-d)^2\right) = 0 \tag{35}$$

$$(y(a-b) + d(x-a))\,(x^2 + y^2) + ay\left((x-b)^2 + (y-d)^2\right) = 0\,, \tag{36}$$

which can be solved under $b \neq a/2$ and $d \neq 0$:

$$x_{01,02} = \frac{d(a^2 + 2ab - 8b^2) \pm q(3b^2 - d^2 + p)}{3(a-2b)(2d \mp q)} \tag{37}$$

$$y_{01,02} = (2d \mp q)/6 \qquad \text{with} \tag{38}$$

$$p = \sqrt{(a^2 - ab + b^2 + d^2)^2 - 3a^2 d^2}\ , \quad q = \sqrt{2(d^2 - a^2 + ab - b^2 + p)}\,. \tag{39}$$

The c-values of (32) can be chosen in such a way that $\mathbf{x}_{01}$ or $\mathbf{x}_{02}$ are points of the surfaces

$$c_{01,02}^6 = \prod_{i=1}^{3} (\mathbf{x}_{01,02} - \mathbf{x}_i)^2.$$

Let c_{01} be the smaller value. The surface splits into three different ovals around the three foci for $c < c_{01}$. For $c = c_{01}$ two ovals touch one another in $\mathbf{x}_{01}$ and this joint part grows further with increasing c and touches the third oval in $\mathbf{x}_{02}$ for $c = c_{02}$. This situation is shown in Fig. 9, 10, 13, and 14 for an isosceles triangle of the foci, and in Fig. 17 for an irregular triangle.

If the three foci are collinear ($d = 0$, a case not solved by (37) and (38)) then the contact points are points of the line of the foci: $y_{01} = y_{02} = z_{01} = z_{02} = 0$ and the condition

$$\mathbf{grad}\, f^2(x,y,z) = \mathbf{grad}\, \left((x^2 + y^2 + z^2)\left((x-a)^2 + y^2 + z^2\right)\left((x-b)^2 + y^2 + z^2\right) - c^6\right) = \mathbf{0}$$

is reduced to

$$\frac{df^2(x,0,0)}{dx} = 2x(x-a)(x-b)\left((x-a)(x-b) + x(x-b) + x(x-a)\right) = 0\,.$$

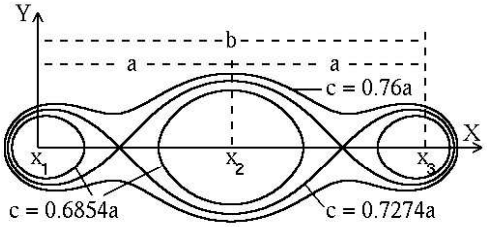

Figure 11: ($z=0$)-cuts of product surfaces with three foci on a line

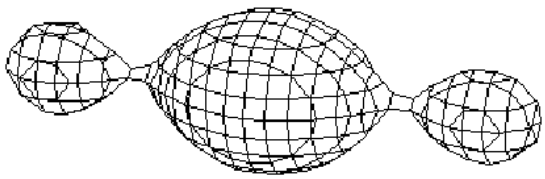

Figure 12: 3D-view of the c_0-surface of Fig. 11

Apart from the three foci ($x_1 = 0$, $x_2 = a$, $x_3 = b$) the solutions of this equation are the contact points

$$x_{01,02} = \tfrac{1}{3}\left(a + b \pm \sqrt{a^2 + b^2 - ab}\right).$$

Figs. 11 and 12 show the surface for equidistant foci $b = 2a$ with the contact points

$$x_{01,02} = a\left(1 \pm \frac{1}{\sqrt{3}}\right)$$

and the common constant

$$c_0^6 = \prod_{i=1}^{3}(x_{01,02} - x_i)^2 = \tfrac{4}{27}\,a^6, \quad \text{i.e.,} \quad c_0 = 0.7274..\,a\,.$$

The last symmetrical case ($b = \frac{a}{2}$), which was not solved by Eqs. (37) and (38), represents an isosceles triangle and splits into three subcases. If one chooses the axis of symmetry of the triangle as the y-axis, i.e., $\mathbf{x}_1 = (-a, 0, 0)$, $\mathbf{x}_2 = (a, 0, 0)$ and $\mathbf{x}_3 = (0, d, 0)$ (see Fig. 9), then the solutions for the contact points are:

$$\begin{aligned}
x_{01,02} &= \pm\tfrac{1}{3}\sqrt{3a^2 - d^2}, & y_{01} &= y_{02} = \tfrac{d}{3}, & &\text{for} \quad d < a\sqrt{3}\,,\\
x_0 &= 0, & y_0 &= \tfrac{d}{3}, & &\text{for} \quad d = a\sqrt{3}\,,\\
x_{01} &= x_{02} = 0, & y_{01,02} &= \tfrac{1}{3}(d \pm \sqrt{d^2 - 3a^2}), & &\text{for} \quad d > a\sqrt{3}\,.
\end{aligned}$$

In the first subcase ($d < a\sqrt{3}$) the angle of the triangle at the focus $\mathbf{x}_3$ is larger than $60°$, $|\mathbf{x}_1 - \mathbf{x}_3| = |\mathbf{x}_2 - \mathbf{x}_3| < |\mathbf{x}_1 - \mathbf{x}_2|$ (see Fig. 13). The ovals around the foci $\mathbf{x}_1$ and $\mathbf{x}_2$ grow with c and get in contact to the third oval simultaneously for

$$c_{01}^6 = c_{02}^6 = \tfrac{4}{27}\,a^2(a^2 + d^2)^2\,.$$

Figs. 13 and 14 show this subcase for a rectangular triangle ($d = a$, $c_0^6 = \frac{16}{27}\,a^6$, $c_0 = 0.9164..\,a$). One can call the c_0-curve a *trifocal lemniscate*.

In the second subcase ($d = a\sqrt{3}$) the three foci create an equilateral triangle with edges of length $2a$. The three ovals meet in the center $\mathbf{x}_0 = \sum \mathbf{x}_i/3$ of the triangle for $c_0^6 = \frac{64}{27}\,a^6$, $c_0 = 1.1547..a$. The ($z=0$)-intersection with the c_0-surface is a lemniscate with three bows (i.e., "lemnis") (see Fig. 15 and 16). In Fig. 18 the same focal triangle is used, but the surface is rendered for $c = c_1$.

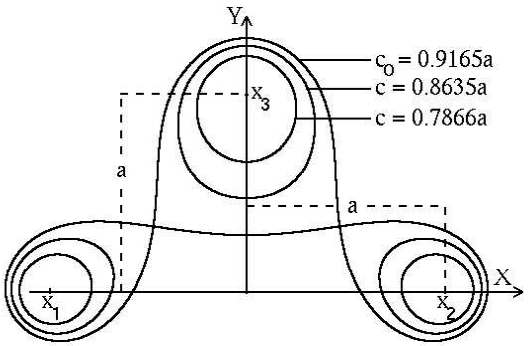

Figure 13: Trifocal lemniscate with a rectangular arrangement of the foci

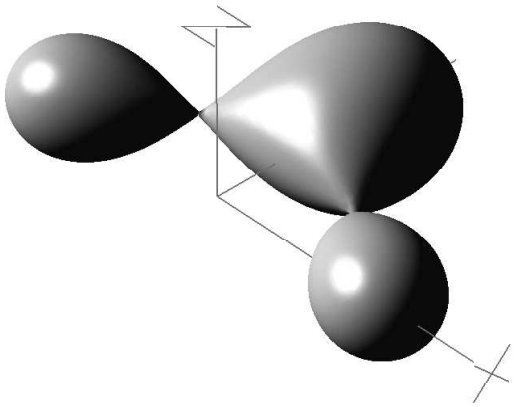

Figure 14: 3D-view of the c_0-lemniscate surface of Fig. 13

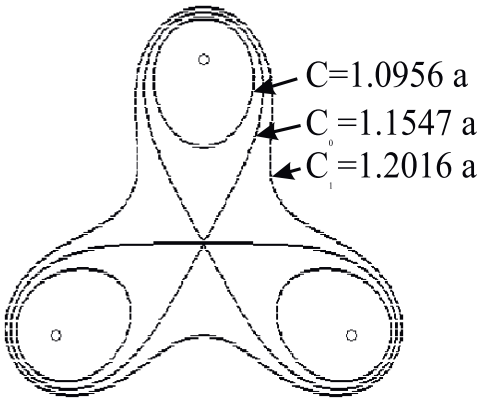

Figure 15: $(z=0)$-cuts of product surfaces with an equilateral focal triangle (32)

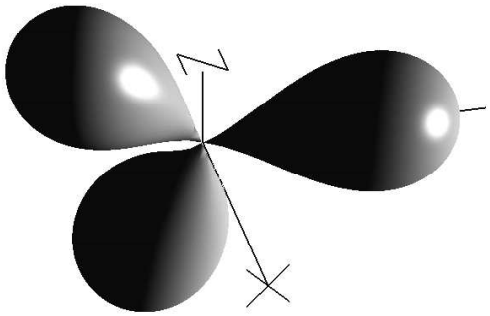

Figure 16: 3D-view of the c_0-surface of Fig. 15

In the last subcase $d > a\sqrt{3}$ the angle at $\mathbf{x}_3$ of the isosceles triangle is acute. Therefore the ovals around $\mathbf{x}_1$ and $\mathbf{x}_2$ melt together on the y-axis in y_{01} for $c = c_{01}$ and this joint part of the surface grows further with c until it meets the third part in y_{02} for $c = c_{02}$ (see Figs. 9 and 10). The c_0-values are

$$c^6_{01,02} = \frac{4}{3^6}\left(d^3 + 9a^2 d \mp \sqrt{d^2 - 3a^2}^3\right)^2 .$$

Fig. 9 displays $(z=0)$-intersections of the example $d = a\sqrt{7}$ with

$$\begin{aligned} y_{01} &= a(\sqrt{7}-2)/3 = 0.2152504\,a\,, & y_{02} &= a(\sqrt{7}+2)/3 = 1.5485838\,a\,, \\ c^6_{01} &= 6.467\,a^6, & c^6_{02} &= 13.90\,a^6 \end{aligned}$$

and a wire frame model of the c_{02}-surface is displayed in Fig. 10.

For large values of c and finite $|\mathbf{x}_i|$ every trifocal product surface becomes a sphere with a radius $|\mathbf{x}| \to c$ according to (32).

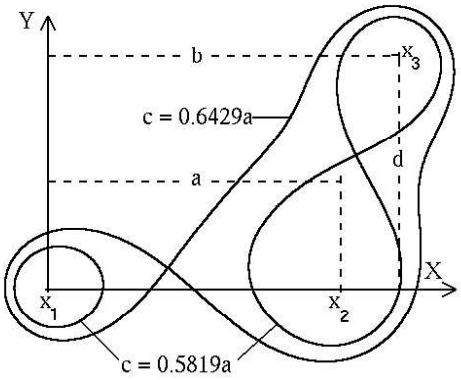

Figure 17: ($z=0$)-cuts of a product surface where the foci form an irregular triangle

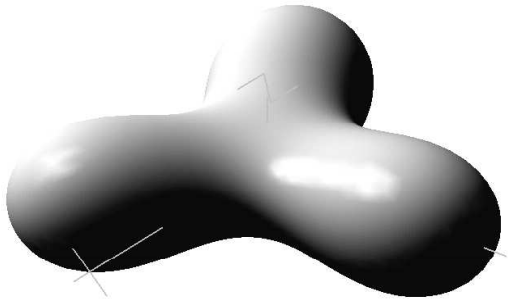

Figure 18: 3D-view of the c_1-surface of Fig. 15 [9]

3.2. Multifocal product surfaces

In this subsection three surfaces are studied. The foci are arranged like the vertices of a tetrahedron, of an octahedron or simply of a *square*

$$\mathbf{x}_{1,2} = (\pm a,\, 0,\, 0), \quad \mathbf{x}_{3,4} = (0,\, \pm a,\, 0)$$

(see Fig. 19). The corresponding product surface

$$\begin{aligned} f \;\; = \;\; & \sqrt{(x-a)^2+y^2+z^2}\cdot\sqrt{(x+a)^2+y^2+z^2}\cdot \\ & \cdot\sqrt{x^2+(y-a)^2+z^2}\cdot\sqrt{x^2+(y+a)^2+z^2} = c^4. \end{aligned} \tag{40}$$

is a biquartic

$$f^2 = \left((x^2+y^2+z^2+a^2)^2-4x^2a^2\right)\left((x^2+y^2+z^2+a^2)^2-4y^2a^2\right) = c^8 \tag{41}$$

which can be written in an explicit form:

$$z = \pm\sqrt{-x^2-y^2-a^2+\sqrt{2(x^2+y^2)a^2+\sqrt{c^8+4a^4(x^2-y^2)^2}}}\,. \tag{42}$$

The surface does not have four contact points at the middle of the sides of the square $(\pm a/2,\, \pm a/2,\, 0)$, as it would be expected, but the origin is the only contact point with $c_0 = a$ (see Fig. 19). The surface looks like Fig. 16, but with four instead of three "clubs".

In general four foci form an irregular tetrahedron and the singular points of the corresponding product surface have to be computed numerically. In the case of a *symmetrical tetrahedron* (see Figs. 21 to 26) with an equilateral triangle as a base and with the top of the tetrahedron on the axis of symmetry z:

$$\mathbf{x}_i = \left(-\tfrac{a}{2}\sqrt{3},\, -\tfrac{a}{2},\, 0\right), \quad \left(\tfrac{a}{2}\sqrt{3},\, -\tfrac{a}{2},\, 0\right), \quad (0,a,0), \quad (0,0,b)$$

the singular points can be calculated analytically. In this case the function of (32) — with four foci — has to be expanded:

$$\begin{aligned} F(x,y,z) = f^2(x,y,z) \;\; = \;\; & \left((x^2+y^2+z^2+a^2+ay)^2-3x^2a^2\right)\cdot \\ & \cdot\left(x^2+(y-a)^2+z^2\right)\left(x^2+y^2+(z-b)^2\right) = c^8. \end{aligned} \tag{43}$$

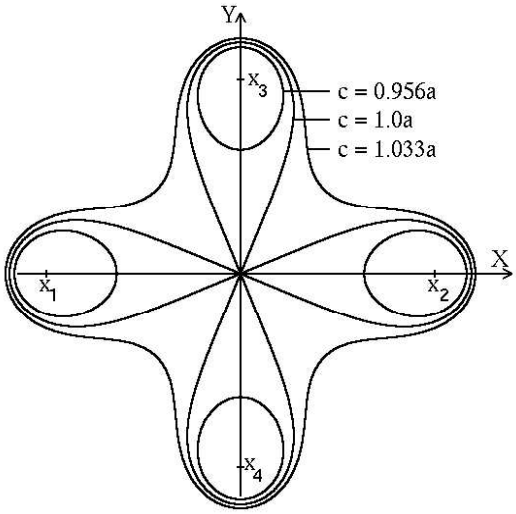

Figure 19: $(z=0)$-cuts of product surfaces where four foci form a square

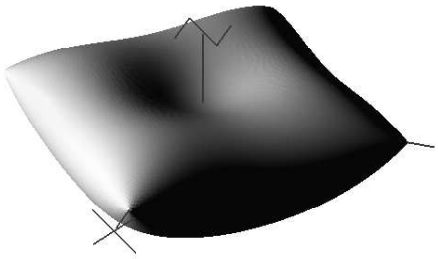

Figure 20: String surface of Fig. 7 with a "repulsive" focus on the z-axis

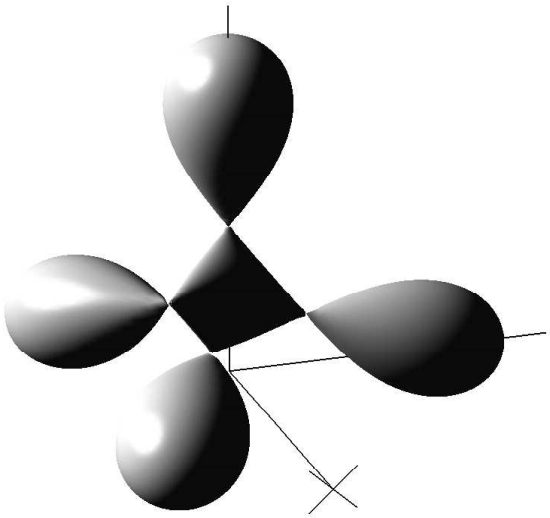

Figure 21: A tetrahedral product surface in the moment of contact of the oval of the pseudofocus in the center with the ovals of the four foci

Figure 22: Coastal tetrapod with $c^8 = 2.5\,a^8$ and $b = a\sqrt{2}$

The surface is shown in Fig. 21 for a regular tetrahedron ($b = a\sqrt{2}$ and $c_{02}^8 = 1.6875\,a^8$). For small c-values it splits into four parts, one oval around each focus. There is a c-value where a fifth oval starts to grow around the center of the tetrahedron: $\mathbf{x}_0 = \left(0,\, 0,\, \frac{b}{4}\right)$. This singular point $\mathbf{x}_0$ is called a *pseudofocus* in this paper, because it has the same characteristics as a focus: $\mathbf{grad}\, F = \mathbf{0}$ and F has according to the theorem of J.J. Sylvester [14] a local

minimum in $\mathbf{x}_0$ because Hesse's determinant and its subdeterminants are positiv:

$$D_1 = \det(F_{11}) > 0 \qquad D_2 = \det\begin{pmatrix} F_{11} & F_{12} \\ F_{21} & F_{22} \end{pmatrix} > 0 \qquad D_3 = \det\begin{pmatrix} F_{11} & F_{12} & F_{13} \\ F_{21} & F_{22} & F_{23} \\ F_{31} & F_{32} & F_{33} \end{pmatrix} > 0\,.$$

Hence the second order term of the Taylor expansion (see (34)) is positive definite. The foci and the pseudofoci differ in their F-values. The F-function has an absolute minimum $F = 0$ in a focus according to Eq. (32) and a pseudofocus is defined as a point of a relative minimum with a positive F-value.

Due to the symmetry of the surface the pseudofocus in the center and the contact point where this fifth oval of the pseudofocus meets the fourth oval of $\mathbf{x}_4$ are singular points on the z-axis:

$$\frac{\partial F(0,0,z)}{\partial z} = \frac{\partial}{\partial z}\left((a^2+z^2)^3(z-b)^2\right) = 2(z-b)(a^2+z^2)^2\left(3z(z-b)+a^2+z^2\right) = 0\,. \quad (44)$$

The fourth focus ($z_4 = b$) is always a solution of this equation. The other two solutions are $z_{01,02} = (3b \pm \sqrt{9b^2-16a^2})/8$. For a regular tetrahedron ($b = a\sqrt{2}$) these values are $z_{01} = b/4$ and $z_{02} = b/2$ the values of the pseudofocus and of the contact point. Eq. (43) gives the c-values of product surfaces, which contain these points: $c^8_{01} = 1.60180\,a^8$ — the F-value for which the oval of the pseudofocus starts to grow — and $c^8_{02} = 1.6875\,a^8$ for the contact-surface.

Here some of the second partial derivatives are zero for points of the z-axis $(0,0,z)$ of the symmetrical tetrahedron, $F_{12} = F_{13} = F_{23} = 0$, while the diagonal elements of Hesse's subdeterminants are simple polynomials

$$\begin{aligned} F_{11}(0,0,z) &= F_{22}(0,0,z) = 2(a^2+z^2)\left((a^2+z^2)^2+3z^2(b-z)^2\right) \\ F_{33}(0,0,z) &= 2(a^2+z^2)\left(a^4+a^2(3b^2-18bz+17z^2)+z^2(15b^2-42bz+28z^2)\right). \end{aligned} \quad (45)$$

The numerical results for the singular points of the z-axis are listed in Table 1. One can see that F has minima in the focus and the pseudofocus because the conditions of Sylvesters theorem are fulfilled.

Table 1: Hesse's determinants for $x = y = 0$

point	z	$F_{11} = F_{22} = D_1$	F_{33}	D_2	D_3
focus	$\sqrt{2}$	54	54	54^2	54^3
contact point	$\sqrt{2}/2$	9	$-9/2$	9^2	$-3^6/2$
pseudofocus	$\sqrt{2}/4$	$3^5/2^6$	$3^5/2^6$	$3^{10}/2^{12}$	$3^{15}/2^{18}$

Because of the symmetry of the surface there are corresponding contact points on the three lines from the center to the foci 1, 2 and 3. For larger c-values (e.g., $c^8 = 2.5\,a^8$) the surface resembles the concrete tetrapods used to reinforce coastlines (see Fig. 22).

With $b = \frac{4}{3}a$ the tetrahedron is not as high as the regular one and both singular points, i.e., the pseudofocus and the contact point coincide:

$$z_{01} = z_{02} = \frac{3}{8}b\,, \quad c^8_{01} = c^8_{02} = \frac{5^5}{2^8 3^2}\,a^8 = 1.3563\,a^8\,.$$

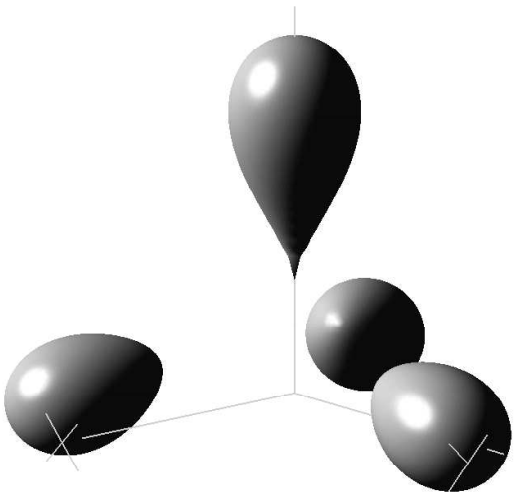

Figure 23: Oval with an apex with $b = \frac{4}{3}\,a$, $c^8 = 1.3563\,a^8$ in Eq. (43)

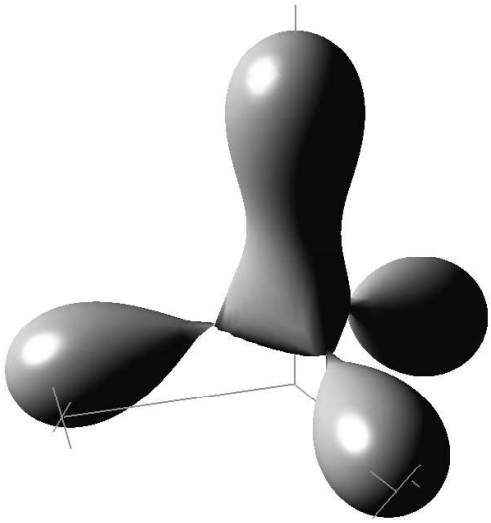

Figure 24: Product surface of Fig. 23 with $c^8 = 1.485\,a^8$

The oval of the fourth focus touches with an apex the "pseudofocus" (see Fig. 23).With increasing c the surface gets the shape of a pacifier for babies until it has contact to the ovals of the other foci simultaneously (see Fig. 24).

Figs. 25 and 26 show the situation when the tetrahedron is higher than a regular one:

$$b = 2a, \quad z_{0i} = \frac{a}{4} \cdot \left(3 \pm \sqrt{5}\right), \quad c_{01}^8 = 3.64385\,a^8\,, \quad c_{02}^8 = 9.53973\,a^8\,.$$

The first three ovals meet in z_{01} (see Fig. 25) and this joint part meets the fourth oval in z_{02} (see Fig. 26).

In a last product surface which was studied the six foci

$$\mathbf{x}_i = (\pm a, 0, 0), \quad (0, \pm a, 0), \quad (0, 0, \pm a)$$

(see Figs. 27 and 28) are the vertices of a *regular octahedron*. Squaring its equation $\prod_{i=1}^{6} |\mathbf{x} - \mathbf{x}_i| = c^6$ leads to the formula

$$\begin{gathered} h(x,y,z) = [q^4 - 4x^2a^2] \cdot [q^4 - 4y^2a^2] \cdot [q^4 - 4z^2a^2] = c^{12} \\ \text{with} \quad q^4 = (x^2 + y^2 + z^2 + a^2)^2. \end{gathered} \tag{46}$$

It is symmetrical with respect to a permutation of the three axes. The plotting algorithms of Section 5 shows that for small c-values there exist seven ovals, one around each focus and one around the origin which acts again like a pseudofocus. Because of the symmetry the contact points lie on the axes, e.g., on the x-axis and are determined by the equation

$$\frac{\partial h(x,0,0)}{\partial x} = \frac{\partial}{\partial x}\left(((x^2 + a^2)^2 - 4x^2a^2)(x^2 + a^2)^4\right) = 0 \tag{47}$$

which corresponds to (33). The foci $x = \pm a$ and the contact points $x_{01,02} = \pm a/\sqrt{3}$ are solutions of this equation. The same points are found on the y- and z-axis (see Fig. 28).

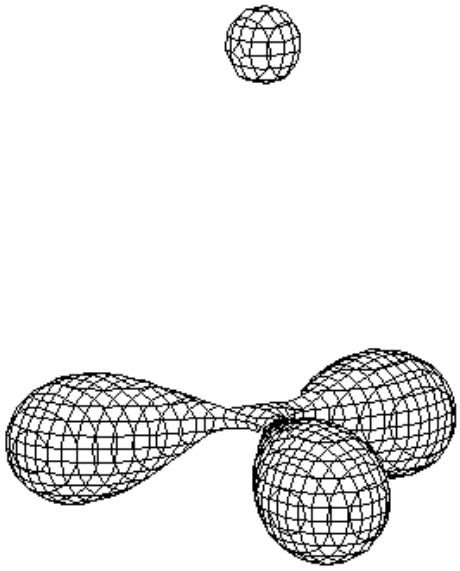

Figure 25: Product surface of a long tetrahedron where three ovals get contact: $b = 2a$, $c^8 = 3.678\,a^8$

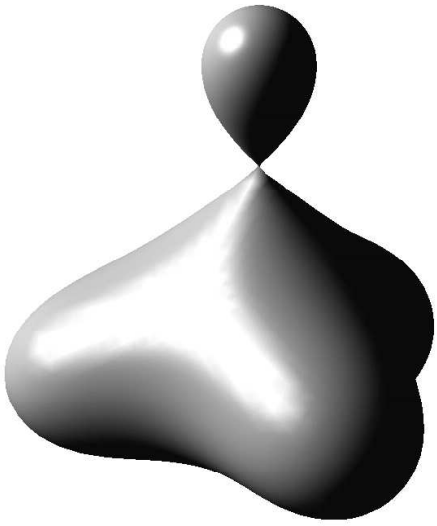

Figure 26: Focal arrangement as in Fig. 25 but with $c^8 = 9.6\,a^8$

Eq. (46) gives the c-values of the moment of contact: $c_0 = a\sqrt[6]{\frac{32}{27}} = 1.0287212\,a$. The oval around the origin vanishes with decreasing c (before the ovals around the foci do so for $c = 0$) because the origin is an isolated point of the $(c{=}a)$-surface (see (46)). Therefore the surface has six parts only in the parameter interval $0 \le c < a$ and seven parts for $a \le c < c_0$ which melt together for $c = c_0$.

A parameter representation of (46) is possible by the introduction of spherical polar coordinates $(x = r\cos\theta\sin\phi, \quad y = r\sin\theta, \quad z = r\cos\theta\cos\phi)$:

$$\begin{aligned} \phi &= \pm\arcsin\sqrt{A/B} \\ A &= c^{12} - (r^2+1)^6 + 4(r^2+1)^4 r^2 - 4r^4(r^2+1)^2\sin^2 2\theta \\ B &= 4r^4\cos^2\theta((r^2+1)^2\cos^2\theta - r^2\sin^2 2\theta). \end{aligned} \tag{48}$$

One can prevent the ovals around the foci from getting direct contact to one another in the center of the surface as shown in Fig. 16 and 19 or to a "pseudofocus" in the center (see Figs. 21, 28) by placing a focus with a negative exponent in the center $\mathbf{x}_0$:

$$F(x,y,z) = f^2(x,y,z) = \frac{1}{(\mathbf{x}-\mathbf{x}_0)^{2k}}\prod_{i=1}^{n}(\mathbf{x}-\mathbf{x}_i)^2 = c^{2(n-k)}. \tag{49}$$

If all the $|\mathbf{x}_i|$ are finite and if $\mathbf{x}_i \neq \mathbf{x}_0$ for $i = 1, 2, \ldots, n$ then there are no points of a surface with finite c in the neighbourhood of $\mathbf{x}_0$ because F becomes very large for $\mathbf{x} \to \mathbf{x}_0$.

In Fig. 29 the same six foci $\mathbf{x}_i$ as in Fig. 28 and their function h of (46) are used and in addition a focus $\mathbf{x}_0$ with a negative exponent is placed in the center ($\mathbf{x}_0 = \mathbf{0}$, $k = 4$, $a = 1$, $c^4 = 13.0403$):

$$h(x,y,z)/\mathbf{x}^8 = c^4. \tag{50}$$

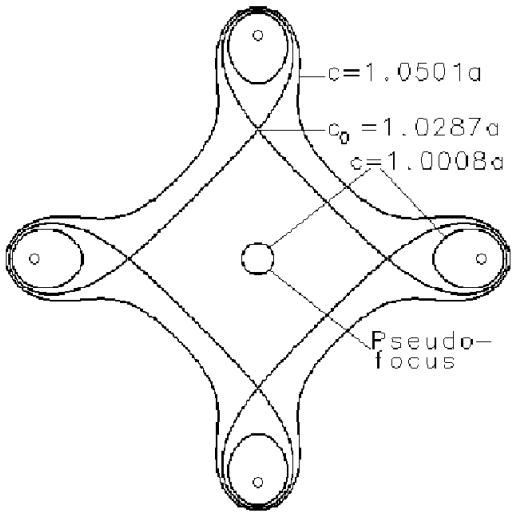

Figure 27: $(z=0)$-cuts of octahedral product surfaces

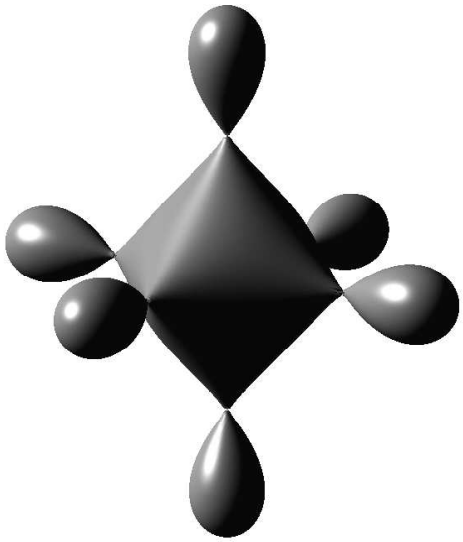

Figure 28: 3D-view of the c_0-surface of Fig. 27

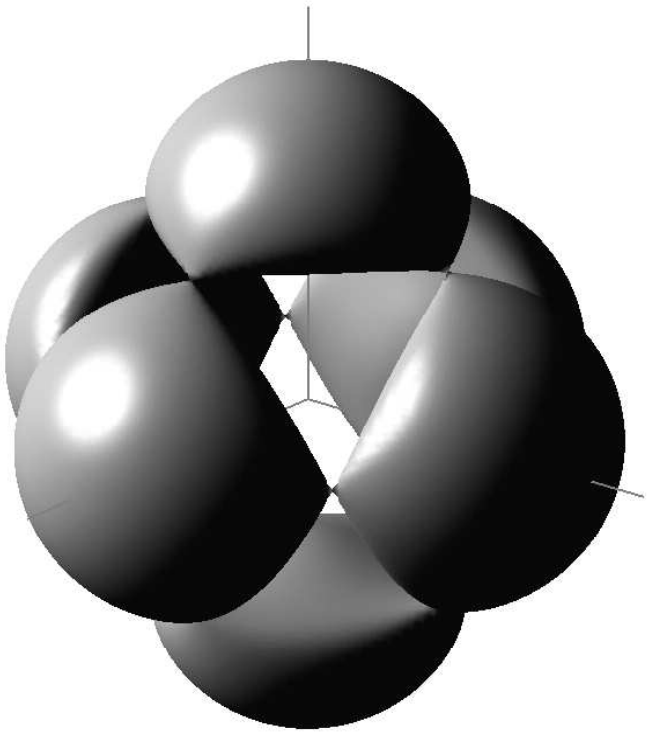

Figure 29: Hollow "octahedron"

This surface has "triangular" holes near the space diagonals, i.e., around the centers of the eight triangles forming the octahedron of the foci. The six foci of the octahedron are inside the six "bubbles". The holes disappear with increasing c and the surface splits into an exterior and an interior part. With (49) it is easy to construct the corresponding surfaces

with holes for the other product surfaces.

One can blow up the oval of a focus $\mathbf{x}_i$ at the expense of the size of the other ovals by counting the focus twice, i.e., by doubling its positive exponent in (32).

4. Axial product surfaces

Fig. 15 shows $(z=0)$-cuts of surfaces which differ in their c-value. One can construct a new surface out of these curves by putting one $(z=0)$-cut above the other in z-direction and by changing the c-values with z:

$$f(x,y)=\prod_{i=1}^{n}\sqrt{(x-x_i)^2+(y-y_i)^2}=c^n(z). \tag{51}$$

By this procedure the foci $\mathbf{x}_i$ move up in z-direction along "focal axes" (x_i,y_i,z). The product of (51) is constant for constant z and the distances $|\mathbf{x}-\mathbf{x}_i|$ are "horizontal" lines parallel to the $(z=0)$-plane. Fig. 30 shows such a function for $n=3$. It looks like a triple hammer. With the foci of an equilateral triangle

$$\mathbf{x}_1=\left(-a,\,-\frac{a}{\sqrt{3}},\,0\right),\quad \mathbf{x}_2=\left(a,\,-\frac{a}{\sqrt{3}},\,0\right),\quad \mathbf{x}_3=\left(0,\,\frac{2a}{\sqrt{3}},\,0\right)$$

Eq. (51) yields

$$f^2(x,y)=\left((x^2+y^2+a^2+ya)^2-3x^2a^2\right)\left(x^2+(y-a)^2\right)=c^6(z). \tag{52}$$

A "fourfold hammer" is created by:

$$\left((x^2+y^2+a^2)^2-4x^2a^2\right)\left((x^2+y^2+a^2)^2-4y^2a^2\right)=c^8(z). \tag{53}$$

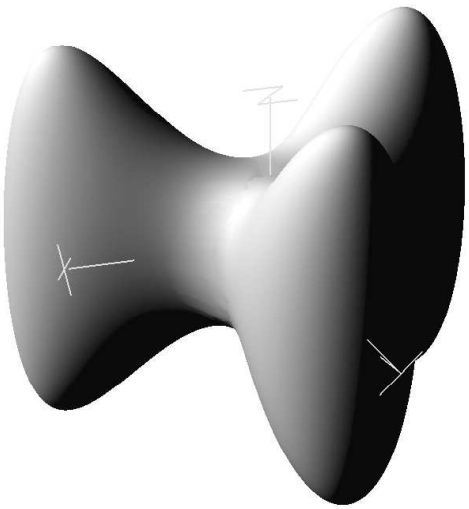

Figure 30: The "triple hammer" with three focal axes

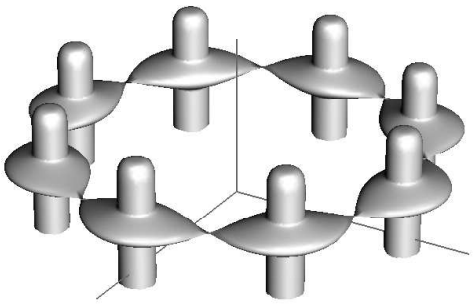

Figure 31: A circle of columns

The parameter interval of $c^n(z)$ is chosen in such a way that it contains small c-values, where the product curve of (51) splits into separate ovals, i.e., it should contain the $(c=0)$-point. The c_0-curve, where the different ovals get into contact, becomes the curve of the saddle point of the new surface, and the region with $c > c_0$ defines the radial size of the central part (see Figs. 15 and 30).

A linear function $c^n(z)$ will produce a surface with sharp tips. The function displayed in Fig. 30 has an elliptical $c^n(z)$-function:

$$\left(\frac{c^n}{1.1\,a^n}\right)^2 + \left(\frac{z}{a}\right)^2 = 1, \qquad c^n = 1.1a^n\sqrt{1-\left(\frac{z}{a}\right)^2} \tag{54}$$

with $n = 3$. A periodical $c^n(z)$-function repeats the surface in z-direction.

In Fig. 31 the surface of an "eightfold hammer" with eight focal axes x_i ($n = 8$ in Eq. (51))

$$F(x,y) = (w^4 - 4x^2a^2)(w^4 - 4y^2a^2)\left(\left(w^4 - 2a^2(x^2+y^2)\right)^2 - 16x^2y^2a^4\right) = c^{16}(z) \tag{55}$$

with $w^4 = (x^2+y^2+a^2)^2$ was changed by the introduction of a focus with a negative exponent in the central axis ($x_0 = y_0 = 0$) as in Eqs. (49) and (50), which forces the eight ovals to get contact to their neighbours (and not to the central axis as in Fig. 30):

$$F(x,y)/(x^2+y^2)^4 = c^8(z) \tag{56}$$

with

$$c^8(z) = \begin{cases} 0.6 \cdot \sqrt{1-\left(\dfrac{z-0.7}{0.1}\right)^2} & \text{for } 0.7 < z \le 0.8 \text{ (the caps of the columns),} \\ 0.6 + 3.6 \cdot \sin^2\left(\dfrac{z-0.2}{15.7079}\right) & \text{for } 0.2 < z < 0.4 \text{ (the ring structure),} \\ 0.6 & \text{else (the columns).} \end{cases}$$

Of course, one can also use helical axes $\mathbf{x}_i(\phi(z))$ or toroidal axes $\mathbf{x}_i(\theta,\phi)$ (or both) with periodical c^n-functions to create nets.

5. Algorithms to display implicit surfaces

Many algorithms are known in Computer Graphics which allow the user to display surfaces given as an explicit function $z = f(x,y)$ or as a parameter representation $\mathbf{x}(u,v)$. During the last two decades two main algorithms were developed to draw implicitly given surfaces $f(x,y,z) = 0$ (see references [3] to [7] and [9] to [13]).

The first one called *"tracked partitioning"* starts with finding a single point $\mathbf{x}_0$ of the surface ($f(\mathbf{x}_0) = 0$) which is chosen as a center of a small cube. Some of the corners of this cube will be inside the surface ($f < 0$) and some of them will be outside ($f > 0$). The continuous surface ($f = 0$) cuts some of the edges of the cube and the algorithm has to find these zeros $\mathbf{x}_k$ with $f(\mathbf{x}_k) = 0$ by recursive bisectioning of the edges. Assuming that the cube is small enough there will be at most one point $\mathbf{x}_k$ on an edge. The method to form a 3D-polygon from these points $\mathbf{x}_k$ is called *polygonization* and is described in the literature [3, 12, 13]. Since a cube has 8 corners there are $2^8 = 256$ possibilities to distribute the signs of f over the corners. Lorensen and Cline [11] reduced all these cases to 14 cases to find the 3D-polygon around the cube. After the polygon is drawn the edges of all adjacent cubes of the

same small size are scanned for zeros of f and care is taken that every cube is processed only once. The algorithm stops if all cubes cutting the surface are found. A program published in [10] is an implementation of this algorithm.

The second algorithm called *"converged partitioning"* is a recursive octree algorithm which starts with a large root cube, checks the sign of f at the corners of its eight octants and calls those octants recursively where corners with different polarities of f occur. Octants where the sign of f does not change are neglected because they are all inside ($f < 0$) or outside ($f > 0$) of the cube. The algorithm stops when the octants reach a minimal size. Then the zeros $\mathbf{x}_k$ of f on the edges of the octants are calculated by recursive bisectioning and a 3D-polygon is constructed as within the "tracked partitioning"-algorithm.

A 2D-simplification of this polygonization process was used in the present paper to draw the wire frame models (e.g. Figs. 10, 12 and 25). It could be used in the "tracked partitioning" algorithm as well. The zeros $\mathbf{x}_k$ which are visible are projected to the projection plane where they represent a two-dimensional set (x'_k, y'_k). The convex hull of this set is computed, sorted to form a ring, closed $(x'_{n+1},\ y'_{n+1}) = (x'_1,\ y'_1)$, and plotted. It is this simple method of the convex hull which solves all the possible cases of polygons discussed in [3], [11] and [12]. It works even well if the surfaces have "bottle necks" as, e.g., in Figs. 10, 12 and 25. The wire frame models of this paper are produced by this method of a 3D-octree with a 2D-polygonization. The observer gets a good impression of the 3D-structure of the surfaces because the polygons show the cuts $x = \text{const}$, $y = \text{const}$ and $z = \text{const}$ (see, e.g., Figs. 12 and 25) since the octree algorithm starts with root cubes which are parallel to the axes. This feature is lost if the polygons are triangulated as in [10]. It is also possible to triangulate the 2D-polygon of the convex hull and to use its 3d-coordinates $\mathbf{x}_k$ to draw Gouraud- or Phong-shaded models of implicit surfaces.

There are surfaces where one visible part of the surface hides another visible part of it (see Fig. 30). To produce good pictures of such surfaces too it is necessary to call those octants first which are more remote from the observer and to erase the inside of the wireframe faces by filling them with the background colour. If the octree-procedure has to be started separately with different root cubes for isolated parts of the surface the remote root cubes have to be called first (see Fig. 29 and 31).

For the shaded models of this paper a new method of *"radial projection"* was developed to display the surfaces. Jackie Neider et. al. [16] described a method of approximating a sphere by a set of triangles. They start with the triangles of an icosahedron considered as a rough approximation of a sphere and subdivide them recursively into smaller triangles which are shaded and displayed. We modified this method to draw an implicit surface $f(x, y, z) = 0$ and enclosed the surface in one or several projection spheres, for which the centers $\mathbf{x}_{ci}$ and the radii R_i have to be defined. The surfaces of these spheres are approximated by an icosahedron or an octahedron á la Jackie Neider and recursively split into smaller triangles. When the triangulation is fine enough a radial search for the zeros $\mathbf{x}_k$ with $f(\mathbf{x}_k) = 0$ starts from every corner $\mathbf{x}_t$ of a triangle. The zeros have to be found on the radial line from the center $\mathbf{x}_{ci}$ to the corner $\mathbf{x}_t$. By this procedure the pattern of triangles of the spheres is projected onto the implicit surface $f = 0$, shaded and displayed.

This method works well for the simple, convex string surfaces. Fermat's point $\mathbf{x}_0$ is chosen as the center $\mathbf{x}_{ci}$ of the projection sphere and the radius R_i has to be large enough that the surface is enclosed in the sphere. Some of the product surfaces (see Figs. 18 and 22) could be drawn in the same way by the use of one projection sphere only, but most of them needed more than one.

To draw the "ring of columns" (see Fig. 31) one needs one sphere per column with a center on the axis of the column and a radius chosen so large that the next contact points are points of the surface of the sphere. Every bubble of the "octahedron" (see Fig. 28) and of the "hollow octahedron" (see Fig. 29) is enclosed in a separate projection sphere. For the "triple hammer" (see Fig. 30) we used three spheres which overlapped one another in the saddle point of the "hammer". In such a case some of the triangles $\mathbf{x}_t$ of the spheres, which should be projected onto the surface, are inside the hammer ($f(\mathbf{x}_t) < 0$) and the radial search does not find a root $\mathbf{x}_k$ with $f(\mathbf{x}_k) = 0$ because the center of the spheres is always inside the surface ($f < 0$) too. In this case the points $\mathbf{x}_t$ of the projection sphere were used as roots $\mathbf{x}_k$. These triangles are inside the "triple hammer" and are drawn in spite of being invisible. They are hidden later on when OpenGL draws the other visible parts of the surface.

6. Conclusions

This article investigates higher order generalisations of the ellipse called "string surfaces" and of the lemniscate called "product surfaces" with regard to their dependence on the arrangement of the foci and on the values of their free constant c. The influence of factors with negative exponents on the design of product surfaces is studied. Analytical and graphical results show that some of these iso-surfaces have corners (see Figs. 2, 3 and 5). The polygonization used in the algorithm simplifies the procedure to draw implicit surfaces and the introduction of product surfaces offers new possibilities to work with skeletons and implicit surfaces. A new method of radial projection is developed and applied to display them.

Acknowledgements

The author likes to thank G. Franke, Fachhochschule Giessen, for the implementation of Linux, F90 and OpenGL and his assistance in using Linux. Some of the calculations were done with the program Mathematica.

References

[1] E. Weiszfeld: *Sur le point pour lequel la somme des distances de n points donnés est minimum.* Tohoku Math. J. **43**, 355–386 (1937).

[2] P. Erdös, I. Vincze: *On the Approximation of Convex, Closed Plane Curves by Multifocal Ellipses.* J. Appl. Probab., spec. vol. **19A**, 89–96 (1982).

[3] J. Bloomenthal (ed.): *Introduction to Implicit Surfaces.* Morgan Kaufmann Publ., San Francisco 1997.

[4] A. Ricci: *A Constructive Geometry for Computer Graphics.* The Computer Journal **16**, no. 2, 157–160 (1973).

[5] C.M. Hoffmann: *Geometric and Solid Modeling.* Morgan Kaufmann Publ., San Mateo 1989.

[6] J.F. Blinn: *A Generalisation of Algebraic Surface Drawing.* ACM Transactions on Graphics **1**, no. 3, 235–256 (1982).

[7] J. Bloomenthal, K. Shoemake: *Convolution Surfaces.* Computer Graphics **25**, no. 4, 251–255 (1991).

[8] W.M. Pieper: *Recursive Gauss Integration*. Commun. Numer. Meth. Engng. **15**, 77–90 (1999).

[9] H. Schweissguth: *Darstellung beliebiger mathematischer Flächen der Form $f(x, y, z) = 0$ mit Hilfe eines rekursiven, adaptiven Schattierungsverfahrens*. Diploma Thesis, FH Giessen-Friedberg, FB MNI, 1995.

[10] J. Bloomenthal: *An Implicit Surface Polygonizer*. In P. Heckbert (ed.): *Graphic Gems IV*. Academic Press, London 1994, 324–350.

[11] W.E. Lorensen, H.E. Cline: *Marching Cubes: A High Resolution 3D Surface Construction Algorithm*. Computer Graphics **21**, no. 4, 163–169 (1987).

[12] A. Watt, M. Watt: *Advanced Animation and Rendering Techniques*. Addison Wesley, Reading, MA, 1993.

[13] M.F.W. Schmidt: *Modellierung und Approximation von Kurven und Flächen in impliziter Darstellung*. PhD-Thesis, Technische Hochschule Darmstadt 1992, Shaker Verlag, Aachen 1993.

[14] K. Strubecker: *Einführung in die höhere Mathematik, Vol. IV*. Oldenbourg Verlag, München, Wien 1984.

[15] J. Bloomenthal, B. Wyvill: *Interactive Techniques for Implicit Modeling*. Computer Graphics **24**, no. 2, 109–116 (1990).

[16] J. Neider, T. Davis, M. Woo: *OpenGL Programming Guide*. Addison Wesley, Reading, MA, 1993.

Received September 19, 2001; final form May 22, 2006